Above-threshold ionization, energy-resolved photoelectron angular distributions, and momentum distributions of H_2^+ in intense femtosecond laser pulses

J. Fernández and L. B. Madsen
Lundbeck Foundation Theoretical Center for Quantum System Research, Department of Physics and Astronomy, Aarhus University, 8000 Aarhus C, Denmark
(Received 14 April 2009; published 11 June 2009)

We study above threshold ionization, energy-resolved photoelectron angular distributions and photoelectron momentum distributions for the initial $^2\Sigma_g^+(1s\sigma_g)$ ground and the $^2\Sigma_u^+(2p\sigma_u)$ first-excited state in H_2^+, driven by an arbitrary orientated linearly polarized 800 nm laser pulse of different intensities and temporal durations. When the pulse duration is reduced, multiphoton structure is erased, and continuum states of gerade (g) and ungerade (u) inversion symmetry start to overlap. A strong localization of the photoelectron emission occurs as a consequence of the g-u mixing. Furthermore, as the pulse length is reduced, effects of the carrier-envelope phase show up, and a number of complicated interference patterns in the momentum distribution radially as well angularly are predicted. Such patterns were previously reported in the atomic case. In the molecules, additional structures appear due to the interference between electronic waves emerging from different nuclear centers.

DOI: 10.1103/PhysRevA.79.063406 PACS number(s): 33.80.Rv, 33.20.Xx, 02.70.Hm

I. INTRODUCTION

The hydrogen molecular ion is the simplest molecule and as such has been the favorite of theorists in investigations of molecular effects in strong-field physics. Despite its simplicity, carrying only a single electron and two nuclei, the system has resisted fully *ab initio* descriptions in the regime where most interesting strong-field phenomena occur, i.e., femtosecond pulses of a wavelength of 800 nm, and intensities around 10^{14} W/cm^2. The highly nonlinear interaction with the electromagnetic field simply implies that the full problem with all electronic and nuclear degrees of freedom is too numerically demanding to be solved in the foreseeable future: the full problem of dissociative ionization is still largely open. As a consequence the computational models applied to this problem are accurate either in the nuclear part, i.e., dissociation, or in the electronic part, i.e., ionization.

We have recently developed computational models to address the electronic part in fully three dimensions, keeping the nuclei fixed at their equilibrium positions [1,2]. Within this approximation effects of orientation on the ionization can be studied by the rotation of the direction of the polarization vector with respect to the molecule. A few other groups have also been able to compute these effects (see, e.g., Refs. [3,4] and references therein). However, in our approach, we describe the continuum dynamics of the electron in an angle- and energy-resolved way, allowing us to study the ionization process at the most detailed level of momentum distributions. Recall that single ionization is the first step in strong-field phenomena involving rescattering, such as enhanced ionization, high-harmonic generation (HHG), or plateau in above threshold ionization (ATI). Fully understanding this step is accordingly important.

In the present work, we investigate effects of pulse duration and carrier-envelope phase (CEP). The investigation of these effects is timely in view of progress in laser technology. With current technology, one can generate femtosecond (fs) laser pulses with few optical cycles [5,6]. The peak electric field of such few-cycle pulses depends on the CEP, which specifies the delay between the maximum of the envelope and the nearest maximum of the electric field of the carrier wave with frequency ω_0 (see Fig. 1). Since the ionization process depends on the field in a highly nonlinear way, the asymmetry of the field induces an asymmetry in the emission direction of photoelectrons [7–18]. Note that including nuclear motion is far beyond the scope of the present work. We expect the typical effect of nuclear motion to be a smearing out of the reported features [19].

The purpose of the present paper is twofold. First, we study the role of the pulse duration on ATI, molecular frame photoelectron angular distributions (MFPADs), and momentum distributions of H_2^+, in the fixed nuclei approximation, for intensities ranging from 5×10^{13} to 5×10^{14} W/cm^2. Second, we investigate to what extend the CEP can be used to control the electron emission. We focus on H_2^+ because it represents a useful workbench on which to test different approaches and numerical methods. Moreover, experiments us-

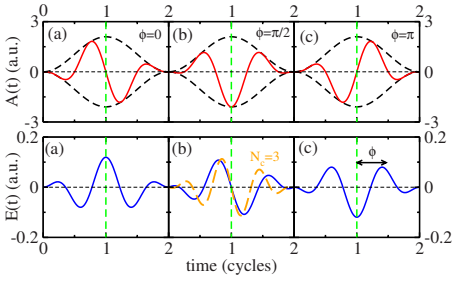

FIG. 1. (Color online) Upper panels, vector potential $A(t)$ and its envelope (dashed line) and, lower panels, electric field $E(t)$ as a function of time in cycles for three values of the CEP, ϕ: (a) 0; (b) $\pi/4$; (c) $\pi/2$. The laser field corresponds to an 800 nm pulse of 2 optical cycles and intensity 5×10^{14} W/cm^2. The vertical dashed lines give the maximum of the envelope. An optical cycle corresponds to 110.2 a.u. (2.7 fs). In panel (b), lower row, we include a rescaled electric field of a 3 optical cycle laser pulse.

ing H_2^+ beams have been performed (see, e.g., Refs. [20–22] and references therein).

The paper is organized as follows: in Sec. II, we introduce our methodology [1,2,23]. Next, in Sec. III we present results for ATI spectra, MFPADs, and electron momentum distributions for the $^2\Sigma_g^+(1s\sigma_g)$ ground and the $^2\Sigma_u^+(2p\sigma_u)$ first-excited state. For the ground state and intensities 3×10^{14} and 5×10^{14} W/cm^2, the roles of the pulse duration and CEP are presented in Secs. III A and III B, respectively. Results for the $^2\Sigma_u^+(2p\sigma_u)$ first-excited state using intensities in the range 5×10^{13}–5×10^{14} W/cm^2, are presented in Sec. III C. Finally, conclusions and future perspectives are given in Sec. IV. Atomic units ($m_e=\hbar=|e|=a_0=1$) are used throughout unless stated otherwise.

II. THEORY AND COMPUTATIONAL DETAILS

In this section we sketch a recently introduced methodology [1,2]. The method for solving the time-dependent Schrödinger equation (TDSE) was described previously [23–26]. In short, for a fixed internuclear distance, and a given orientation of the polarization vector with respect to the molecular axis, β, the wave packet describing the electron dynamics is expanded in terms of spherical harmonics, $\Psi(\boldsymbol{r},\beta,t)=\Sigma_{\ell,m}^{\ell_{\max}} r^{-1} f_{\ell,m}(r,\beta,t) Y_\ell^m(\hat{\boldsymbol{r}})$, In our case, we consider the nuclear equilibrium distance of 2 a.u., and use an expansion with $\ell_{\max}=23$, and a sphere of radius $R_{\max}=600$ a.u. divided into 4096 radial grid points, i.e., step-size, $\Delta r\simeq0.14$ a.u. The TDSE is solved by means of the split-step method, using a time step of $\delta t=0.005$ a.u. Here we employ the velocity gauge of the electron-field interaction, since this gauge has proved superior to the length gauge with respect to the number of angular momenta needed for convergence, and since we are not interested in dynamics during the laser pulse [27,28].

We consider a linearly polarized few-cycle pulse in the dipole approximation wherein the incident field $\boldsymbol{E}(t)=-\partial_t \boldsymbol{A}(t)$ is defined through the vector potential

$$\boldsymbol{A}(t)=A_0(t)\sin[\omega_0(t-T/2)+\phi]\boldsymbol{e}_z \tag{1}$$

for $0\le t\le T$, and zero outside this interval, where T is the duration of the pulse, and $\boldsymbol{e}_z$ is the unit vector along the z axis in the laboratory frame. We consider a sine-square envelope function $A_0(t)=A_0\sin^2(\omega_0 t/2N_c)$ that assumes its maximum at $t=T/2$ (see upper panels of Fig. 1). In Eq. (1), ϕ is the CEP that specifies the delay between this maximum of the envelope and the nearest maximum of the electric field of the carrier wave with frequency ω_0. Figure 1 illustrates our definition of the CEP: For $\phi=0$, maxima of field and envelope coincide [panel (a)], while for $\phi=\pi/2$ the maximum of the envelope coincides with the zero of the field. Therefore, $\phi=0$ and $\phi=\pi/2$ (modulo π) correspond to cosine and sine pulses with respect to the maximum of the envelope. We consider the angular frequency $\omega_0=0.057$ a.u. corresponding to a central wavelength of 800 nm. In this work, we consider four different pulse durations ~19, 13, 8, and 4 fs, corresponding to $N_c=7$, 5, 3, and 2 optical cycles, respectively, and we consider the intensities, 5×10^{13}, 1×10^{14}, 3×10^{14}, and 5×10^{14} W/cm^2, in order to reflect different physical mechanisms.

After the laser field is turned off, the fully differential ionization probability, differential in (i) the electron energy, ε, (ii) the emission direction in the molecular frame, $\Omega_e=(\theta_e,\phi_e)$, and (iii) the polarization direction, β, is obtained from the wave packet $\Psi(\boldsymbol{r},\beta,T)$ by [1,2,23]

$$\frac{dP(\beta)}{d\Omega d\varepsilon}=\left|\sum_\mu i^{-\ell}e^{i\sigma_\ell(\varepsilon)}I_\mu(\varepsilon,\beta)Y_\ell^{\Lambda*}(\Omega_e)\right|^2. \tag{2}$$

Here the summation index μ denotes the set of quantum numbers $\mu=\{\Lambda,\pi,\ell\}$, where Λ is the value of the z component of the total electronic angular momentum $(\Sigma,\Pi,\ldots)$, π denotes the symmetry under inversion (g or u) and ℓ designates the asymptotic electronic angular momentum of a continuum state with given Λ and symmetry π. Without loss of generality we consider the polarization vector to be contained in the xz molecular plane. In Eq. (2), $\sigma_\ell(\varepsilon)$ is the Coulomb phase shift for partial wave ℓ, and $I_\mu(\varepsilon,\beta)$ is the matrix element

$$I_\mu(\varepsilon,\beta)=\langle\psi_\mu^-(\boldsymbol{r})|\Psi(\boldsymbol{r},\beta,t=T)\rangle, \tag{3}$$

where $\psi_\mu^-(\boldsymbol{r})$ represents a continuum (scattering) state of the field-free molecular Hamiltonian of energy ε with incoming wave boundary conditions [29,30], and asymptotic momentum $\boldsymbol{k}$.

The continuum states needed for projection are obtained in a B-splines basis set [31,32], applying the method developed in Refs. [33,34]. In our case, scattering states with quantum numbers $^2\Lambda_{g/u}$ up to $|\Lambda_{\max}|=23$ are described by a partial wave expansion, ℓ, of 12 terms (see Refs. [1,2] for more details). Note that in the special case of a laser field linearly polarized along the molecular axis, i.e., $\beta=0$, the axial symmetry is preserved, and therefore only the $^2\Sigma_{g/u}^+$ symmetries are accessible. In this case 24 partial waves in Eq. (2) are sufficient. For an arbitrary oriented laser polarization as considered in this work, the existence of a component of the electric field perpendicular to the molecular axis breaks the axial symmetry, so that the angular momentum projection Λ is no longer conserved, and for this case the coherent interference of 576 partial waves has to be considered.

From Eq. (2) we obtain the (angle-integrated) ATI spectrum:

$$\frac{dP(\beta)}{d\varepsilon}=\int_0^{2\pi}\int_0^{\pi}\frac{dP(\beta)}{d\Omega d\varepsilon}\sin\theta d\theta d\phi=\sum_\mu|I_\mu(\varepsilon,\beta)|^2. \tag{4}$$

Comparing Eqs. (2) and (4), we see that only the angle differential quantity of Eq. (2) is sensitive to the phase shifts of the continuum wave functions, since Eq. (4) is an incoherent sum of norm squares of matrix elements.

III. RESULTS

We use the methodology outline above to study the role of the pulse duration and the CEP on ionization of H_2^+ initialized from the ground- or the first-excited state.

A. Role of the pulse duration

In this section, we present the results of the ionization of the H_2^+ molecule from the $^2\Sigma_g^+(1s\sigma_g)$ ground state focusing

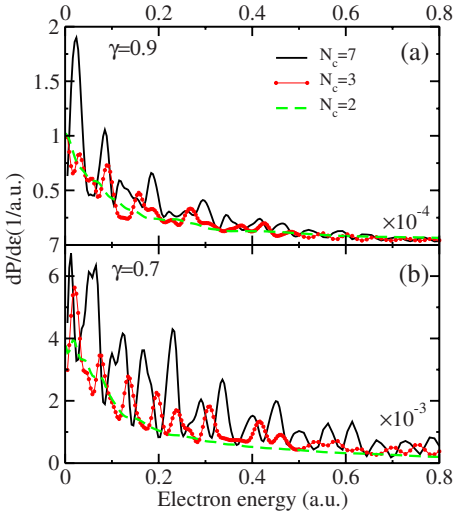

FIG. 2. (Color online) ATI spectrum of H_2^+ for $\beta=0°$ driven by an 800 nm laser pulse, with $\phi=0$ and two different intensities (a) 3×10^{14} and (b) 5×10^{14} W/cm^2, as a function of the number of optical cycles, $N_c=7,5,2$. The Keldysh parameter, γ, is shown in each panel. The small numbers in the lower right of each panel indicate the factor by which the results should be multiplied to obtain the true value of the ionization probability.

on the role of the pulse duration in the ATI spectrum, the energy-resolved MFPAD, and the photoelectron momentum distribution.

1. Above-threshold ionization and photoelectron angular distributions

Results for the ATI spectrum [Eq. (4)] of H_2^+ starting out in the ground state are given in Fig. 2, for the parallel geometry, $\beta=0°$, an 800 nm laser pulse, $\phi=0$ in Eq. (1) and intensities (a) 3×10^{14} and (b) 5×10^{14} W/cm^2, and three pulse durations, $N_c=7$, 5 and 2. At 800 nm an optical cycle corresponds to 110.2 a.u. (2.7 fs). For both intensities, results obtained with a laser pulse of $N_c=7$ optical cycles display the typical ATI spectra characterized by a series of peaks separated from each other by the energy corresponding to the angular frequency of the carrier. In each panel, we include the Keldysh parameter [35], $\gamma=\sqrt{I_p/2U_p}$, where I_p is the ionization potential ($I_{1s\sigma_g}(R_{\rm eq})=1.10237$ a.u. and $I_{2p\sigma_u}(R_{\rm eq})=0.66753$ a.u.), and $U_p=I/4\omega_0^2$ is the ponderomotive energy with I the peak intensity of the field in atomic units.

As the duration of the pulse is reduced, for a given laser intensity, (i) the ATI peaks are drastically washed out, (ii) the signal is reduced, and (iii) the energy positions of the ATI peaks are shifted. These effects are well known and can be understood considering the time-energy uncertainty principle, $\Delta t\Delta E\geq\hbar/2$: as the duration of the pulse is reduced, the pulse is spectrally broadened and neighboring peaks will begin to overlap and interfere. Basically, a given final kinetic energy can be reached through more than a single energy-absorption pathway involving different numbers of absorbed photons. Alternatively, we may think of the two-cycle data as the result of a series of electric-field bursts in different directions. In each half-cycle an electronic wave packet is launched. Wave packets launched by different half-cycles may subsequently interfere [36,37].

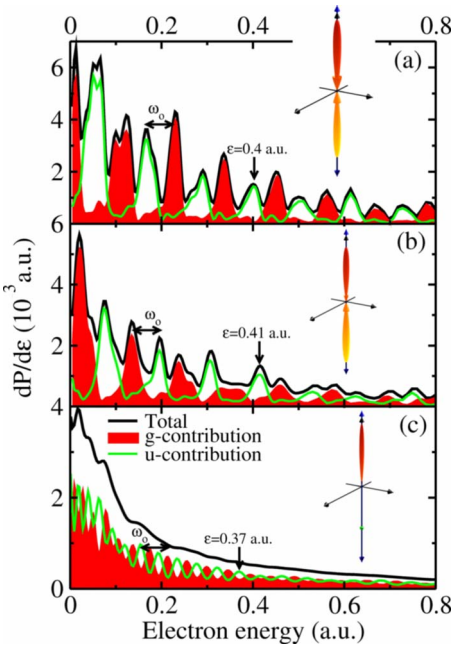

FIG. 3. (Color online) Inversion symmetry decomposition (gerade-ungerade) of the ATI spectrum of H_2^+ for $\beta=0°$ driven by an 800 nm laser pulse of $I=5\times10^{14}$ W/cm^2, $\phi=0$, and three different numbers of optical cycles, (a) $N_c=7$, (b) 5, and (c) 2. The energy associated with the angular frequency of the carrier ω_0 is represented by a horizontal double arrow. For the indicated electron energy, ε, the MFPAD is displayed. All three-dimensional (3D) plots are normalized to unity at the maximum of the electron angular distribution. These maxima of the MFPADs are (a) 0.0073, (b) 0.0075, and (c) 0.0113. The molecular axis is placed along the z axis of the molecular fixed frame.

The breakdown of the multiphoton picture may be analyzed further by considering the inversion symmetry decomposition of the ATI spectrum (Fig. 3). Figure 3 shows the ATI spectrum for the parallel geometry (same conclusions can be extracted for other orientations) obtained at 800 nm, 5×10^{14} W/cm^2, and $\phi=0$, for three pulse durations, $N_c=7$, 5, and 2. For pulses with $N_c=7$ and 5 optical cycles, the inversion symmetry character of each ATI peak alternates from peak to peak [Fig. 3(a) and 3(b)]. Contrary, for a pulse of 2 optical cycles [Fig. 3(c)], the g-u decomposition, while still visible, gives contributions of similar magnitude and washes out the ATI spectrum. When both g- and u-type continuum states are populated, an asymmetric photoelectron angular distribution is observed due to interference [MFPAD in Fig. 3(c), see also Ref. [1]]. This latter effect is similar to what is known for bound states. For example, in a double-well potential a linear combination of a delocalized symmetric and antisymmetric state may result in a state localized in one of the wells. In H_2^+ in few cycle, strong fields, the combination of g and u states in the continuum results in a localization of the ejected photoelectrons to a half plane. Note that the g-u-induced localization should not be confused with CEP control over the photoelectron emission. The former is a pure quantum effect giving highly directional pulsed bursts

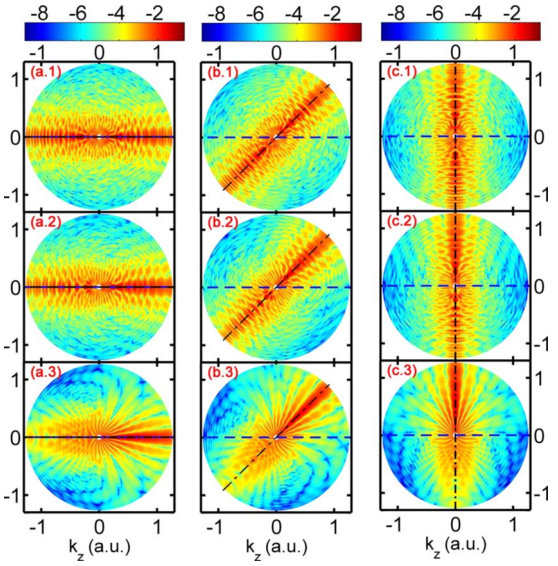

FIG. 4. (Color online) Differential momentum distributions (in logarithmic scale) following strong-field ionization of the ground state of H_2^+ in the k_z-k_x plane for three orientations of the polarization vector (a) $\beta=0°$, (b) 45°, and (c) 90°, and three different number of optical cycles, $N_c=7$ in (a.1, b.1, c.1); $N_c=5$ in (a.2, b.2, c.2) and $N_c=2$ in (a.3, b.3, c.3). The wavelength is 800 nm and the peak intensity is 5×10^{14} W/cm^2. The molecule is placed along the k_z axis (dashed line) and the polarization vector is given by the dash-dotted line.

of electrons at particular energies, while the latter can be understood classically in terms of the simple man's model [see Eq. (5)].

2. Momentum distributions and asymmetry coefficient

A detailed analysis of the electron yield produced by an external laser field can be performed in terms of the triple-differential momentum distribution, $dP/d\boldsymbol{k}=dP/kd\Omega_e d\varepsilon$. Figure 4 shows the results in the k_z-k_x plane, for the following orientations of the polarization vector, (a) $\beta=0°$, (b) 45°, and (c) 90°, driven by an 800 nm laser pulse of intensity 5×10^{14} W/cm^2 and $\phi=0$, for $N_c=7$, 5, and 2 optical cycles, panels labeled (a.1, b.1, c.1), (a.2, b.2, c.2), and (a.3, b.3, c.3), respectively. The results in Fig. 4 are displayed on a logarithmic scale in order to reveal the global angular distribution. For all pulse durations considered the results share some common features: The electrons are preferentially emitted along the polarization vector and, in spite of the different numbers of continuum states (and partial waves) taken into account for each particular orientation, the observed secondary structures are practically independent of β [1].

In Fig. 4, ATI peaks for $N_c=7$ manifest themselves as ringlike structures. For a laser pulse with $N_c=7$ optical cycles [Figs. 4(a.1), 4(b.1), and 4(c.1)], the momentum distribution presents a symmetric distribution with respect to the center of inversion of the molecule. As the pulse duration is reduced, the symmetry of the electron distribution is clearly lost (see also Fig. 3) and the preferred direction of electron emission can be explained classically by assuming that an electron is freed at the peak of the field $t=t_0$ with initial velocity $\boldsymbol{v}(t_0)=\boldsymbol{0}$ and subsequently moves under the influence of the external field only [15,17,18],

$$\boldsymbol{k}_{\text{final}}=-\int_{t_0}^{\infty}\boldsymbol{E}(t')dt'=-\boldsymbol{A}(t_0). \tag{5}$$

Hence, in this simple man's model, the direction of ejection is opposite the direction of the maximum vector potential.

The low-energy electron momentum distributions present stripes fanning out radially from $k=0$. For the extreme case of a pulse of $N_c=2$ optical cycles, these fanlike structures completely dominate the forward electron distribution. So, in contrast to the ($N_c=2$) ATI spectrum, where a lack of structures is more than evident, the momentum distribution clearly displays a number of complicated interference pattern radially as well as angularly in the forward direction at specific position. What is more, the number and angular direction of these jets are independent on β and their widths grow with the electron energy. We have checked that these jets are also present in the results obtained with a laser pulse of an intensity 3×10^{14} W/cm^2 (figure not shown), and in the same angular directions. Similar structures are also observed for the ionization of the H_2^+ molecule from the first-excited state, $^2\Sigma_u^+(2p\sigma_u)$, making use of a laser pulse of a similar time duration and intensity [see Figs. 9(c.4) and 9(d.4)].

Structures in the low k momentum distribution have been intensively studied for atoms experimentally [38,39] as well as theoretically [40–45] and originate from the interaction between the outgoing low-energy electron and the long-range asymptotic Coulomb potential [see, e.g., Figs. 3(d) and 3(c) in Ref. [45]]. Their number depends on the intensity and the binding energy [44], and they tend to be dominated by a single angular momentum. While in the present molecular case, the presence of the long-range monopole is still important to obtain the radial fans, the distributions are no longer dominated by a single angular momentum since for an arbitrary orientation of the polarization vector, many continuum states of different symmetries are accessible, and the contribution of each of them to the ionization process is described by a large number of partial waves. In other words, the angular momentum mixing taking place at short distances due to the multicenter molecular potential impedes a straight forward generalization of the atomic models. The number of jets seems to be larger than what would be expected from the atomic case [40–45], an effect we attribute to the ℓ mixing discussed above, or equivalently, but slightly different phrased, to the interference of waves originating from the two molecular centers.

The observed angular asymmetry in Figs. 3 and 4 can be quantified through the definition of the angular asymmetry coefficient [1,16,18,46–48],

$$A_\beta(\varepsilon)=\frac{P_\beta^+(\varepsilon)-P_\beta^-(\varepsilon)}{P_\beta^+(\varepsilon)+P_\beta^-(\varepsilon)}, \tag{6}$$

where $P_\beta^+(\varepsilon)[P_\beta^-(\varepsilon)]$ is the ionization probability obtained along β, in two opposite directions, $\phi_e=0°(\phi_e=180°)$. Figure 5 shows $A_\beta(\varepsilon)$ for $\beta=0°$ driven by an 800 nm laser pulse of intensity 5×10^{14} W/cm^2, $\phi=0$, and four different num-

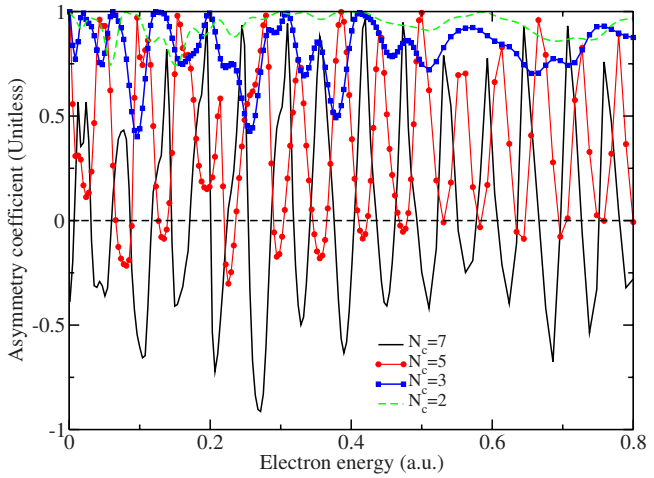

FIG. 5. (Color online) Angular asymmetry coefficient [Eq. (6)] for $\beta=0°$ as a function of the electron energy for four different pulse durations in number of optical cycles, N_c. The wavelength is 800 nm and the peak intensity is 5×10^{14} W/cm^2.

ber of optical cycles, $N_c=7$, 5, 3, and 2. As the pulse duration is reduced, the angular asymmetry approaches unity and decreases its oscillatory character as a function of the electron energy. Only for very low-energy electrons, the position of the minimum and maximum appears at the same electron energy for all the N_c considered, while for higher electron energies the oscillation character is lost.

B. Role of the CEP

Now we focus our attention on the role of changing the CEP in the ionization process from the $H_2^+[^2\Sigma_g^+(1s\sigma_g)]$ ground state.

1. Above-threshold ionization spectra

Figure 6 displays the ATI spectrum of ground state H_2^+ for $\beta=0°$ as a function of the CEP, driven by an 800 nm laser pulse of 3 optical cycles and intensity 5×10^{14} W/cm^2. We choose a 3 optical cycle laser pulse, since CEP effects emerge as the pulse duration is reduced, and at the same time, the ATI spectrum still presents the characteristic multiphoton peaks. As can be seen in Fig. 6, the effect of controlling the CEP presents two main features: as the CEP is varied from 0 to $\pi/2$, (i) the position of a given ATI peak is shifted to higher electron energies, and (ii) its intensity is reduced. The first effect can be qualitatively explained by referring to the simple man's model [Eq. (5)] which also maps the instant of ionization to the final energy of the electron. As the CEP increases from zero for the considered 3 cycle pulse, the peaks of the electromagnetic field change, so t_0 changes such that more energy is picked up from the field. To explain the second effect, we note that as t_0 changes the peaks of the electromagnetic field are effectively reduced and therefore less ionization is observed.

If the CEP is not controlled the "integrated-CEP" ATI spectrum should present wider ATI peaks than the ones obtained for a specific ϕ. Same conclusions can be extracted

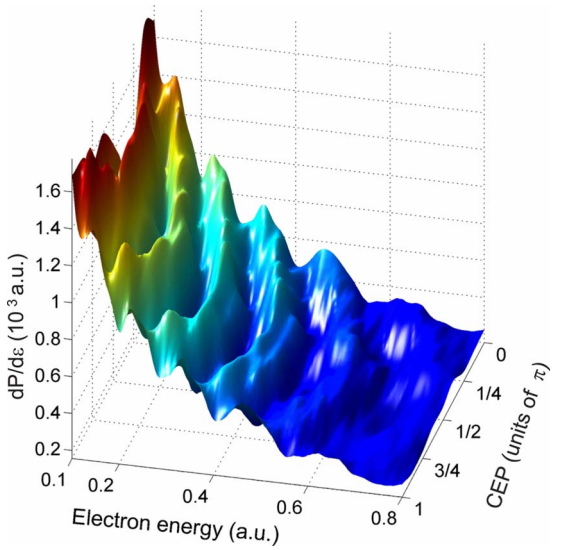

FIG. 6. (Color online) ATI spectrum of H_2^+ initially in the ground state, for $\beta=0°$ as a function of the CEP and the electron energy, driven by a laser pulse with $N_c=3$ optical cycles. The wavelength is 800 nm and the peak intensity is 5×10^{14} W/cm^2.

for other orientations of the polarization vector, β. Due to inversion symmetry the total ionization remains invariant when the CEP is changed by π (or equivalently when the system is rotated by π) for atoms and symmetric molecules interaction with linearly polarized pulses. Therefore, the ATI spectrum is the same for $\phi=0$ and π for all β.

2. Momentum distributions and asymmetry coefficient

Figure 7 shows the momentum distribution following strong-field ionization of the ground state of H_2^+ in the k_z-k_x plane for the orientations $\beta=0°$, 45°, and 90°, panels labeled (a), (b), and (c), respectively, driven by an 800 nm laser pulse of 3 optical cycles and intensity 5×10^{14} W/cm^2, for three values of the CEP, $\phi=0$, $\pi/4$ and $\pi/2$, panels labeled (a.1, b.1,c.1), (a.2, b.2, c.2), and (a.3, b.3, c.3), respectively. The results are presented in logarithmic scale in order to be able to display the different structures. As in Fig. 4, for all CEP, the electron is preferably emitted along the polarization vector, and we also see "jets" symmetrically distributed with respect to the direction of the polarization vector. The number and angular directions of these structures are also similar (compare only results displayed in the first row, $\phi=0$). In Fig. 1(b) we display the rescaled electric field corresponding to a pulse of 3 optical cycles. As can be seen, this pulse and the 2 optical cycles pulse are quite similar, explaining the presence of similar structures in both electron momentum distributions. As the CEP is varied from 0 to $\pi/2$, the main electron emission direction is reversed from forward to backward. Note that the results obtained for $\phi=\pi$ are the specular imagine of the result obtained for $\phi=0$ with respect to k_x axis. The change in the emission direction as ϕ is changed from 0 to π implies a change in the relative phase between states of opposite inversion symmetry. This emission asymmetry can be measured through the asymmetry angular coefficient, making use of Eq. (6).

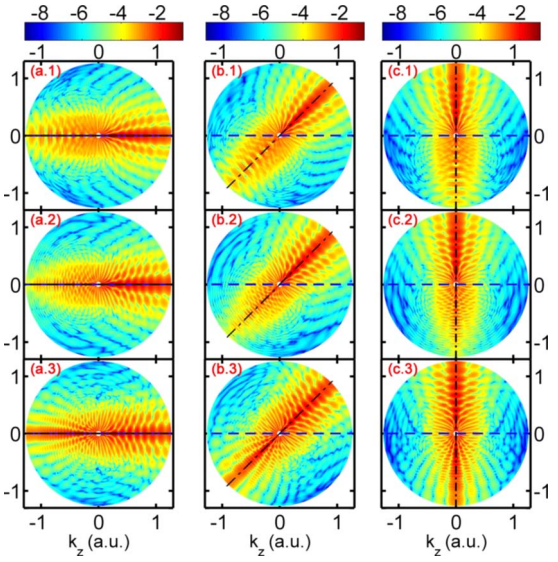

FIG. 7. (Color online) Differential momentum distributions (in logarithmic scale) following strong-field ionization of the ground state of H_2^+ in the k_z-k_x plane for three orientations of the polarization vector (a) $\beta=0°$, (b) 45° and (c) 90° and three values of the CEP, $\phi=0$ in (a.1, b.1,c.1), $\phi=\pi/4$ in (a.2, b.2, c.2), and $\phi=\pi/2$ in (a.3, b.3, c.3). The wavelength is 800 nm and the peak intensity is 5×10^{14} W/cm^2. The molecule is placed along the k_z axis (dashed line) and the polarization vector is given by the dash-dotted line.

Figure 8 shows the angular asymmetry coefficient [Eq. (6)] for ground-state H_2^+ with $\beta=0°$ as a function of electron energy and CEP in an 800 nm laser pulse of 3 optical cycles and intensity 5×10^{14} W/cm^2. Whereas the dependence on the electron energy is relatively weak, the asymmetry coefficient presents a strong dependence varying from 1 to −1 (forward-backward emission) as the CEP is varied from 0 to π. Moreover, the angular asymmetry coefficient displays a $\sim\cos(\phi)$ dependence. Hence, the study of the angular asymmetry coefficient can be used to determined the value of the CEP.

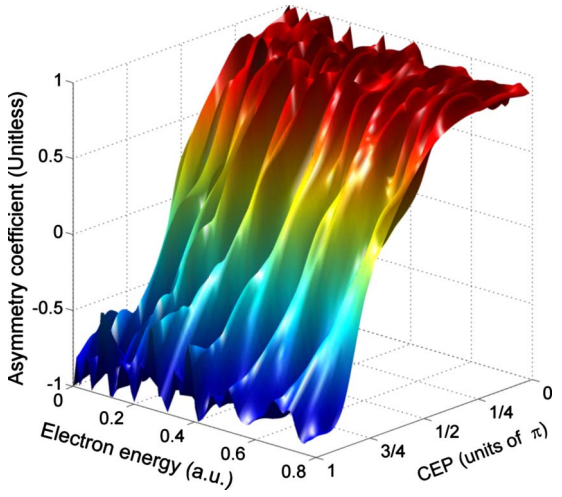

FIG. 8. (Color online) Angular asymmetry coefficient [Eq. (6)] of H_2^+ initially in the ground state for $\beta=0°$ as a function of electron energy and CEP. The field contains $N_c=3$ optical cycles. The wavelength is 800 nm and the peak intensity is 5×10^{14} W/cm^2.

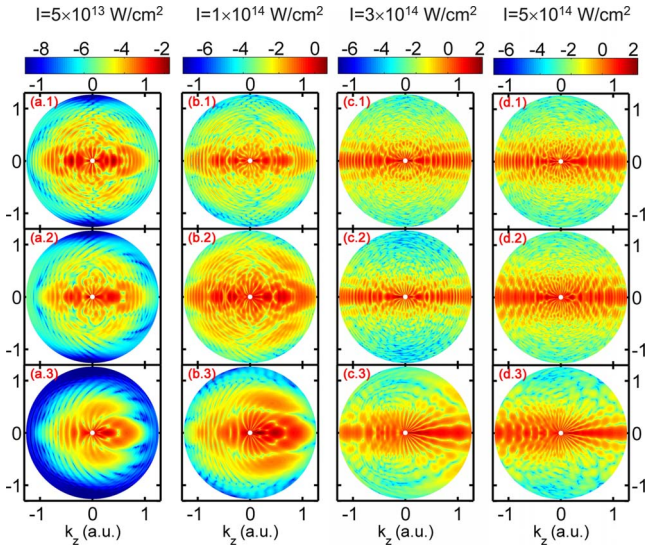

FIG. 9. (Color online) Differential momentum distribution of H_2^+ for the $^2\Sigma_u^+(2p\sigma_u)$ excited state (in logarithmic scale) in the k_z-k_x plane for $\beta=0°$, driven by an 800 nm laser pulse with $\phi=0$, for four different intensities, (a) 5×10^{13}, (b) 1×10^{14}, (c) 3×10^{14}, and (d) 5×10^{14} W/cm^2 and three different numbers of optical cycles, $N_c=7$ in (a.1, b.1, c.1, d.1), $N_c=5$ in (a.2, b.2, c.2, d.2), and $N_c=2$ in (a.3, b.3, c.3, d.3). The molecule and the polarization vector are placed along the k_z axis.

C. $^2\Sigma_u^+(2p\sigma_u)$ excited state

To explore effects related to molecular-state symmetry, we now turn to a discussion of results following strong-field ionization of the first-excited $^2\Sigma_u^+(2p\sigma_u)$ state in H_2^+. Figure 9 displays the two-dimensional momentum distribution in the k_z-k_x plane for a parallel orientation, $\beta=0°$, and an 800 nm laser pulse with $\phi=0$, four different intensities (a) 5×10^{13}, (b) 1×10^{14}, (c) 3×10^{14}, and (d) 5×10^{14} W/cm^2 and three different pulse durations, $N_c=7$, 5 and 2, panels labeled (a.1, b.1, c.1, d.1), (a.2, b.2, c.2, d.2), and (a.3, b.3, c.3, d.3), respectively. Results for other orientations are very close to the ones obtained by a global rotation of the $\beta=0°$ electron momentum distribution. The considered intensities correspond to Keldysh parameters 1.75, 1.23, 0.71, and 0.55, respectively. The photoelectron momentum distributions show surprisingly rich but different structures at the considered intensities. For the lowest intensities in Figs. 9(a) and 9(b) the momentum distributions are dominated by the presence of two circular structures symmetrically distributed with respect to the $k_z=0$. As the pulse duration is reduced, the symmetry of the electron emission is lost, as in Fig. 4, presenting a mainly forward emission direction. What is more, the results driven by a 2 optical cycle pulse present a clear circular structure in the forward direction. Results obtained for the two higher intensities, display similar structures as the ones obtained for the ground state (Fig. 4).

Figure 10 displays the ATI spectrum of H_2^+ obtained from an angular integration of the results shown in Fig. 9. Results obtained for $N_c=7$ and 5, present the normal multiphoton features. Figures 10(a) and 10(b) show that the reduction in the pulse duration from 7 to 5 optical cycles leads to a de-

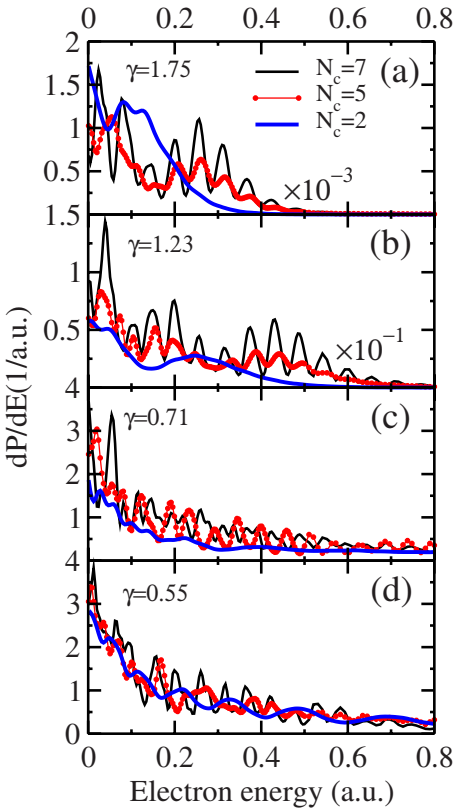

FIG. 10. (Color online) ATI spectrum of H_2^+ from the $^2\Sigma_u^+(2p\sigma_u)$ excited state for $\beta=0°$ driven by an 800 nm laser pulse, $\phi=0$, for four different intensities, (a) 5×10^{13}, (b) 1×10^{14}, (c) 3×10^{14}, and (d) 5×10^{14} W/cm^2 and three different numbers of optical cycles, $N_c=7$, 5, and 2. The Keldysh parameter, γ, is shown in each panel. The small numbers in panels indicate the factor by which the results should be multiplied to obtain the true value of the ionization probability.

crease in the yield, but the number and energy position of each ATI peak remains unchanged. Therefore in this regime, i.e., for pulses that are long enough to show ATI peaks, the ionization process is not that sensitive to the duration of the pulse but mainly to the intensity. ATI peaks reached without the participation of intermediate resonances are known to shift toward lower energies as the intensity grows due to the increase in the ionization potential by U_p. On the other hand, for higher intensity, Figs. 10(c) and 10(d) show patterns similar to the ones previously obtained for the ground state (Fig. 2): the position of the ATI peaks appears at different electron energies, as the pulse duration is reduced. This fact can be explained as an interference of electron wave packets born in successive cycles [36,37]. Therefore, in this regime the pulse duration (number of cycles) plays a crucial role. Note that in this case all peak positions are independent of the intensity. For a pulse of 2 optical cycles, the ATI spectrum obtained for the two lowest intensities presents drastically different features. First, the well-known ATI structure in the electron spectrum is completely erased. Instead, in panel (a) it can be seen that the electron spectrum displays a fast smooth decay from 0 to ~0.5 a.u. and a double peaked structure of width ~0.1 a.u. Beyond this dominant structure the spectrum smoothly decay and goes to zero ~0.4 a.u. In particular, it looks like the double peaked structures are imposed on top of a smoothly decaying background. Increasing the intensity to 1×10^{14} W/cm^2 [panel (b)] implies the shifting to lower electron energies of the double peaked structure, in agreement with a laser-induced shift of the threshold and associated channel closing. As for longer pulse duration, a secondary structure appears at higher electron energies, although in this case it is situated at lower electron energies. Increasing the intensity deep in the tunneling regime [Figs. 10(c) and 10(d)] makes the peak structure less pronounced, similar to the results obtained for the ground state (Fig. 2). In particular, for the higher intensity considered here, the ATI spectrum displays the presence of shallow peaks that are not separated by the photon energy.

IV. SUMMARY AND CONCLUSIONS

In conclusion, our numerical simulations reveal that the photoionization dynamics of even a single-electron molecule near the tunneling regime shows extremely rich and interesting behavior. We have studied the dependence of the ionization of the H_2^+ molecule on the pulse duration and the CEP. For the ground- and the first-excited states, we have observed how the reduction in the pulse duration has three main consequences: first, the erasement of any multiphoton feature in the ATI spectrum. Second, strongly asymmetric electron emission along the polarization vector at particular energies. And third, the appearance of strong radial structures (jets) in the momentum distribution. We have also studied the role of the CEP in the ionization process. We have shown how the CEP can be used to control the population of continuum states and therefore, the electron emission direction.

In this paper, we have focused on the low-energy part of the spectrum, corresponding to direct electrons that are ejected without further interaction with the molecular core, i.e., no rescattering. Beyond the energies of direct electrons, a plateau extends up to energies of $>15U_p$. These electrons are due to rescattering: electrons can scatter elastically from the core after they are driven back by the laser field. After the recollision, the scattered electron is further accelerated by the field and can thus gain a large amount of energy. For molecules, it has been suggested that scattering from more than one nucleus gives rise to a diffraction pattern in the electron angular distribution [49], because the wave packets scattered from different nuclei can interfere constructively or destructively with each other. Therefore, interference effects due to multicenter nature of the problem should appear very clearly for rescattered electrons at higher electron energy. A change in the molecular geometry during the departure in the field would then lead to a change in the electron distribution, so that ATI could be used as a tool to probe nuclear dynamics. Also, in Ref. [50] it was proposed that lasers can be used to produce electron beams *in situ*, which in turn can be used to diffract from their host targets, and that quantitative information on the structure of the host can be extracted form the observed pattern [51]. Interference patterns have been recently described in the one-photon ionization of the simplest diatomic molecules, the H_2^+ and H_2 [52–54]. Ionization of diatomic molecules driven by a laser field at high electron

energies implies a tremendous computational challenge applying the methodology described here, since the number of continuum states that are required to obtain convergence in the high-energy part of the spectrum is much larger that for the lower part (for example, for a parallel orientation, our preliminary calculations required the calculation of continuum states described by more than a hundred of partial waves). Our preliminary results show features similar to the ones observed in the one-photon ionization process [52–54].

ACKNOWLEDGMENT

This work is supported by the Danish Research Agency (Grant. No. 2117-05-0081).

[1] J. Fernández and L. B. Madsen, J. Phys. B **42**, 021001 (2009).
[2] J. Fernández and L. B. Madsen, J. Phys. B **42**, 085602 (2009).
[3] G. Lagmago Kamta and A. D. Bandrauk, Phys. Rev. A **75**, 041401(R) (2007).
[4] D. A. Telnov and Shih-I Chu, Phys. Rev. A **76**, 043412 (2007).
[5] T. Brabec and F. Krausz, Rev. Mod. Phys. **72**, 545 (2000).
[6] F. Krausz and M. Ivanov, Rev. Mod. Phys. **81**, 163 (2009).
[7] E. Cormier and P. Lambropoulos, Eur. Phys. J. D **2**, 15 (1998).
[8] P. Dietrich, F. Krausz, and P. Corkum, Opt. Lett. **25**, 16 (2000).
[9] J. P. Hansen, J. Lu, L. B. Madsen, and H. M. Nilsen, Phys. Rev. A **64**, 033418 (2001).
[10] G. G. Paulus, F. Grasbon, H. Walther, P. Villoresi, M. Nisoli, S. Stagira, E. Priori, and S. D. Silvestri, Nature (London) **414**, 182 (2001).
[11] H. M. Nilsen, L. B. Madsen, and J. P. Hansen, Phys. Rev. A **66**, 025402 (2002).
[12] D. B. Milošević, G. G. Paulus, and W. Becker, Phys. Rev. Lett. **89**, 153001 (2002).
[13] D. B. Milošević, G. G. Paulus, and W. Becker, Phys. Rev. A **71**, 061404(R) (2005).
[14] D. B. Milošević, G. G. Paulus, D. Bauer, and W. Becker, J. Phys. B **39**, R203 (2006).
[15] S. Chelkowski and A. D. Bandrauk, Phys. Rev. A **65**, 061802(R) (2002).
[16] S. Chelkowski and A. D. Bandrauk, Phys. Rev. A **71**, 053815 (2005).
[17] Christian Per Juul Martiny and L. B. Madsen, Phys. Rev. Lett. **97**, 093001 (2006).
[18] C. P. J. Martiny and L. B. Madsen, Phys. Rev. A **76**, 043416 (2007).
[19] S. Barmaki, H. Bachau, and M. Ghalim, Phys. Rev. A **69**, 043403 (2004).
[20] B. D. Esry, A. M. Sayler, P. Q. Wang, K. D. Carnes, and I. Ben-Itzhak, Phys. Rev. Lett. **97**, 013003 (2006).
[21] J. McKenna, A. M. Sayler, F. Anis, B. Gaire, N. G. Johnson, E. Parke, J. J. Hua, H. Mashiko, C. M. Nakamura, E. Moon, Z. Chang, K. D. Carnes, B. D. Esry, and I. Ben-Itzhak, Phys. Rev. Lett. **100**, 133001 (2008).
[22] I. Ben-Itzhak, P. Q. Wang, A. M. Sayler, K. D. Carnes, M. Leonard, B. D. Esry, A. S. Alnaser, B. Ulrich, X. M. Tong, I. V. Litvinyuk, C. M. Maharjan, P. Ranitovic, T. Osipov, S. Ghimire, Z. Chang, and C. L. Cocke, Phys. Rev. A **78**, 063419 (2008).
[23] L. B. Madsen, L. A. A. Nikolopoulos, T. K. Kjeldsen, and J. Fernández, Phys. Rev. A **76**, 063407 (2007).
[24] T. K. Kjeldsen, L. B. Madsen, and J. P. Hansen, Phys. Rev. A **74**, 035402 (2006).
[25] T. K. Kjeldsen, L. A. A. Nikolopoulos, and L. B. Madsen, Phys. Rev. A **75**, 063427 (2007).
[26] L. A. A. Nikolopoulos, T. K. Kjeldsen, and L. B. Madsen, Phys. Rev. A **75**, 063426 (2007).
[27] L. B. Madsen and D. Dimitrovski, Phys. Rev. A **78**, 023403 (2008).
[28] D. Dimitrovski and L. B. Madsen, Phys. Rev. A **78**, 043424 (2008).
[29] G. Breit and H. A. Bethe, Phys. Rev. **93**, 888 (1954).
[30] C. Jungen and D. Dill, J. Chem. Phys. **73**, 3338 (1980).
[31] H. Bachau, E. Cormier, P. Decleva, J. E. Hansen, and F. Martín, Rep. Prog. Phys. **64**, 1815 (2001).
[32] C. de Boor, *A Practical Guide to Splines* (Springer, New York, 1978).
[33] M. Brosolo and P. Decleva, Chem. Phys. **159**, 185 (1992).
[34] M. Brosolo, P. Decleva, and A. Lisini, Comput. Phys. Commun. **71**, 207 (1992).
[35] L. V. Keldysh, Sov. Phys. JETP **20**, 1307 (1965).
[36] S. X. Hu and A. F. Starace, Phys. Rev. A **68**, 043407 (2003).
[37] C. Arendt, D. Dimitrovski, and J. S. Briggs, Phys. Rev. A **76**, 023423 (2007).
[38] A. Rudenko, K. Zrost, C. D. Schröter, V. L. B. de Jesus, B. Feuerstein, R. Moshammer, and J. Ullrich, J. Phys. B **37**, L407 (2004).
[39] C. M. Maharjan, A. S. Alnaser, I. Litvinyuk, P. Ranitovic, and C. L. Cocke, J. Phys. B **39**, 1955 (2006).
[40] Z. Chen, T. Morishita, A. T. Le, M. Wickenhauser, X. M. Tong, and C. D. Lin, Phys. Rev. A **74**, 053405 (2006).
[41] D. G. Arbo, S. Yoshida, E. Persson, K. I. Dimitriou, and J. Burgdörfer, Phys. Rev. Lett. **96**, 143003 (2006).
[42] T. Morishita, Z. Chen, S. Watanabe, and C. D. Lin, Phys. Rev. A **75**, 023407 (2007).
[43] D. G. Arbo, J. E. Miraglia, M. S. Gravielle, K. Schiessl, E. Persson, and J. Burgdörfer, Phys. Rev. A **77**, 013401 (2008).
[44] D. G. Arbo, K. I. Dimitriou, E. Persson, and J. Burgdörfer, Phys. Rev. A **78**, 013406 (2008).
[45] M. Abu-samha, D. Dimitrovski, and L. B. Madsen, J. Phys. B **41**, 245601 (2008).
[46] G. G. Paulus, F. Lindner, H. Walther, A. Baltuška, E. Goulielmakis, M. Lezius, and F. Krausz, Phys. Rev. Lett. **91**, 253004 (2003).
[47] S. P. Goreslavski, G. G. Paulus, S. V. Popruzhenko, and N. I. Shvetsov-Shilovski, Phys. Rev. Lett. **93**, 233002 (2004).
[48] X. M. Tong, K. Hino, and N. Toshima, Phys. Rev. A **74**, 031405(R) (2006).
[49] H. Niikura, F. Légaré, R. Hasbani, A. D. Bandrauk, M. Y. Ivanov, D. M. Villeneuve, and P. B. Corkum, Nature (London) **417**, 917 (2002).

[50] D. Ray, B. Ulrich, I. Bocharova, C. Maharjan, P. Ranitovic, B. Gramkow, M. Magrakvelidze, S. De, I. V. Litvinyuk, A. T. Le, T. Morishita, C. D. Lin, G. G. Paulus, and C. L. Cocke, Phys. Rev. Lett. **100**, 143002 (2008).

[51] T. Morishita, A. T. Le, Z. Chen, and C. D. Lin, New J. Phys. **10**, 025011 (2008).

[52] O. A. Fojón, A. Palacios, J. Fernández, R. D. Rivarola, and F. Martín, Phys. Lett. A **350**, 371 (2006).

[53] J. Fernández, O. Fojón, A. Palacios, and F. Martín, Phys. Rev. Lett. **98**, 043005 (2007).

[54] J. Fernández, O. Fojón, and F. Martín, Phys. Rev. A **79**, 023420 (2009).